Title

Muscle spindle alterations precede onset of sensorimotor deficits in Charcot–Marie–Tooth type 2E

Journal

Genes Brain & Behavior, 16(2)

ISSN

1601-1848

Authors

Villalón, E
Jones, MR
Sibigtroth, C
et al.

Publication Date

2017-02-01

DOI

10.1111/gbb.12341

Peer reviewed

HHS Public Access

Author manuscript

Genes Brain Behav. Author manuscript; available in PMC 2018 February 01.

Published in final edited form as:

Genes Brain Behav. 2017 February ; 16(2): 260–270. doi:10.1111/gbb.12341.

Muscle spindle alterations precede onset of sensorimotor deficits in Charcot-Marie-Tooth type 2E

Eric Villalón[1,2], **Maria R. Jones**[1,2], **Christine Sibigtroth**[3], **Sammy J. Zino**[1,2], **Jeffrey M. Dale**[1,2], **Dan S. Landayan**[4], **Hailian Shen**[5], **DDW Cornelison**[1,2], and **Michael L. Garcia**[1,2,†]

[1]Division of Biological Sciences, University of Missouri-Columbia. Columbia, MO 65211

[2]Bond Life Sciences Center, University of Missouri-Columbia. Columbia, MO 65211

[3]Department of Veterinary Medicine and Surgery, College of Veterinary Medicine, University of Missouri-Columbia, Columbia, MO 65211

[4]Quantitative and Systems Biology, University of California Merced, Merced, CA 95343

[5]Institute of Neuroscience, Shanghai Institutes for Biological Sciences, Chinese Academy of Sciences, Shanghai 200031 China.

Abstract

Charcot-Marie-Tooth (CMT) is the most common inherited peripheral neuropathy, affecting approximately 2.8 million people. CMT leads to distal neuropathy that is characterized by reduced motor nerve conduction velocity, ataxia, muscle atrophy and sensory loss. We generated a mouse model of CMT type 2E (CMT2E) expressing human neurofilament light E396K (hNF-L^{E396K}), which develops decreased motor nerve conduction velocity, ataxia, and muscle atrophy by 4 months of age. Symptomatic hNF-L^{E396K} mice developed phenotypes that were consistent with proprioceptive sensory defects as well as reduced sensitivity to mechanical stimulation, while thermal sensitivity and auditory brainstem responses were unaltered. Progression from pre-symptomatic to symptomatic included a 50% loss of large diameter sensory axons within the fifth lumbar dorsal root of hNF-L^{E396K} mice. Due to proprioceptive deficits and loss of large diameter sensory axons, we analyzed muscle spindle morphology in pre-symptomatic and symptomatic hNF-L^{E396K} and hNF-L control mice. Muscle spindle cross sectional area and volume were reduced in all hNF-L^{E396K} mice analyzed, suggesting that alterations in muscle spindle morphology occurred prior to the onset of typical CMT pathology. These data suggested that CMT2E pathology initiated in the muscle spindles altering the proprioceptive sensory system. Early sensory pathology in CMT2E could provide a unifying hypothesis for the convergence of pathology observed in CMT.

Keywords

Proprioception; Muscle Spindle; Sensory; Charcot-Marie-Tooth; Neurofilament; Peripheral Neuropathy

[†]Correspondence should be addressed to: Michael L. Garcia, University of Missouri, 340C C.S. Bond Life Sciences Center, 1201 Rollins Rd., Columbia, MO 65211, Phone: 573-882-9712, Fax: 573-884-9395, GarciaML@missouri.edu.

Conflict of interest: The authors declare that they have no conflict of interest

Introduction

Charcot-Marie-Tooth (CMT) neuropathies are broadly grouped into demyelinating (CMT type 1), axonal (CMT type 2), or intermediate forms (CMT type 3, type 4 and X-linked) (Fridman *et al.*, 2015). While the specific mutations causing CMT vary, the clinical presentation is very similar between the major types. CMT clinical signs include foot deformities accompanied by progressive muscle weakness and muscle atrophy as well as loss of sensation and altered joint positioning sense (Pareyson *et al.*, 2006). With more than 60 different genes associated with the various types of CMT (Bouhy & Timmerman, 2013), it is unclear how the clinical presentation is similar across CMT types.

CMT patients show signs of sensory dysfunction including loss of vibration and joint position sense progressing to decreased pain and temperature sensation (Szigeti & Lupski, 2009). Vibration and joint position sense are transmitted to the central nervous system by large myelinated axons, which are designated group II and group Ia/b sensory fibers, respectively (Gilman, 2002). In the periphery, receptors that detect vibration sense include Merkel disk receptors, Meissner's corpuscles and pacinian corpuscles, which can also mediate tactile sensation (Gilman, 2002). Joint position sense is sensed by muscle spindles and Golgi tendon organs (Gilman, 2002). Thus, sensory dysfunction could result from pathology within large myelinated axons, peripheral end organs or both. Alterations in sensory nerves preceding the manifestation of sensorimotor dysfunction are commonly observed in rodent CMT models (Achilli *et al.*, 2009, D'ydewalle *et al.*, 2011, Gillespie *et al.*, 2000, Lee *et al.*, 2013, Sereda *et al.*, 1996). Thus, selective loss of large myelinated sensory fibers could be a common site of initial pathogenesis resulting in convergence of clinical phenotypes observed in CMT patients despite the cellular and genetic variability associated with individual CMT types.

CMT type 2E is an axonal form of CMT that was linked to mutations in the neurofilament light gene (*nefl*) (Mersiyanova *et al.*, 2000) Currently, there are 18 mutations located in all domains of NF-L protein linked to CMT type 2E. Patients expressing the glutamate to lysine at amino acid 396 (E396K) mutation presented with typical CMT signs, such as foot deformities, muscle weakness and atrophy, gait ataxia and altered sensation (Züchner *et al.*, 2004). Moreover, analysis of sural nerve biopsies from patients with the E396K mutation revealed reduced axonal diameters with thinner myelin and loss of sensory axons (Züchner *et al.*, 2004). To study the mechanisms of disease pathogenesis, four CMT2E mouse models were generated, expressing human NF-L^{P22S} (Dequen *et al.*, 2010), mouse NF-L^{N98S}, mouse NF-L^{P8R} (Adebola *et al.*, 2015), and human NF-L^{E397K} (Shen *et al.*, 2011) (referred to hereafter as hNF-L^{E396K}, * see explanation in methods section). Transgenic mice expressing hNF-L^{P22S} developed aberrant hind limb posture, gait ataxia and sensorimotor defects (Dequen *et al.*, 2010, Filali *et al.*, 2011). Cellular analyses of hNF-L^{P22S} mice revealed muscle hypertrophy and denervation without motor or sensory axonal loss (Dequen *et al.*, 2010). Mice expressing mNF-L^{N98S} developed aberrant hind limb posture and tremors when lifted by the tail (Adebola *et al.*, 2015). Additionally, mNF-L^{N98S} expression resulted in neurofilament inclusions in motor and sensory cell bodies and reduced axonal diameters (Adebola *et al.*, 2015). mNF-L^{P8R} mice did not develop a phenotype (Adebola *et al.*, 2015).

We generated a transgenic mouse model expressing hNF-L^{E396K} (Shen *et al.*, 2011). hNF-L^{E396K} mice developed aberrant hind limb posture, foot deformities (Shen *et al.*, 2011) and altered gait (Dale *et al.*, 2012). Cellular pathology included distal limb muscle atrophy without denervation and reduced motor axon diameters as well as reduced myelin thickness (Shen *et al.*, 2011).

In this study, we analyzed sensory systems to determine if hNF-L^{E396K} mice developed sensory deficits. Similar to CMT2E patients, symptomatic hNF-L^{E396K} mice developed sensory dysfunction consistent with loss of joint position sense and reduced sensitivity to mechanical stimulation. Sensory axons that relay joint position and vibration sense to the central nervous system are large myelinated group I and group II axons (Casellini & Vinik, 2007, Tourtellotte & Milbrandt, 1998). Therefore, we quantified sensory axons in pre-symptomatic and symptomatic hNF-L^{E396K} mice. Symptomatic hNF-L^{E396K} mice had reduced numbers of large (>5μm) sensory axons. Sensory axon loss together with alterations in joint position sense suggested possible alterations to the proprioceptive sensory system. Consistent with this hypothesis, cross sectional area and volume of muscle spindles were reduced in pre-symptomatic and symptomatic hNF-L^{E396K} mice. Our results suggested that hNF-L^{E396K} mice developed early alterations in sensory systems that precede the onset of motor system pathology (Shen *et al.*, 2011).

Material and Methods

Animals

hNF-L and hNF-L^{E396K} transgenic mice were generated as separate lines on a C57BL/6J background as previously described (Shen *et al.*, 2011). All procedures were in compliance with the University of Missouri Animal Care and Use Committee and with all local and federal laws governing the humane treatment of animals. Equal number of male and female mice was used for all experiments. All experiments were performed during the light phase (7:00 am - 7:00pm) of the light cycle. Previous analyses of hNF-L^{E396K} mice indicated that overt disease phenotype such as, aberrant hind limb posture, foot deformities, and gait alterations initiate at 4-months of age (Dale *et al.*, 2012, Shen *et al.*, 2011). Thus, for this study, 2-month ± 1 week-old mice were considered pre-symptomatic and 6-month ± 1 week-old mice were used considered symptomatic. Mice were housed in microisolator cages (up to 5 per cage) on a 12-h light/dark cycle, and were given food and water *ad libitum*.

* In the original description of this mutation (Züchner *et al.*, 2004), and in previous publications (Butinar *et al.*, 2008, Dale *et al.*, 2012, Shen *et al.*, 2011, Villalon *et al.*, 2015), this mutation was referred to as E397K. However, mouse (GenBank: AAH16436.1) and human NF-L (GenBank: CAA29097.1) protein sequence show that the mutated amino acid is E396 not E397. The mutated amino acid falls within the most highly conserved sequence, KLLEGEE. The penult glutamic acid is the mutated animo acid, which corresponds to position 396. This discrepancy in positioning has not been explained explicitly, but the field has shifted to refer to this mutation as E396K rather than E397K (Berciano *et al.*, 2015, Elbracht *et al.*, 2014, Pisciotta *et al.*, 2015).

Tissue Preparation and Axon Morphological Analysis

2 and 6-month-old mice were perfused intracardially with 4% paraformaldehyde in 0.1 M Sorenson's phosphate buffer, pH 7.2, and postfixed overnight in the same buffer. Fifth lumbar nerve roots were dissected, treated with 2% osmium tetroxide, washed, dehydrated, and embedded in Epon-Araldite resin. Thick sections (0.75 μm) for light microscopy were stained with ρ-phenylenediamine. Cross sections of 5^{th} lumbar sensory axons were analyzed in at least three mice per group. Axonal diameters were measured using the AxioVision Software (Zeiss International). Entire roots were imaged, imaging thresholds were selected individually, and the cross-sectional area of each axon was calculated and reported as a diameter of a circle of equivalent area. Axons were grouped into >5μm or <5μm bins, and were analyzed for statistical significance.

Balance beam

Previous analyses of hNF-L^{E396K} mice indicated that overt disease phenotype such as, aberrant hind limb posture, foot deformities, and gait alterations initiate at 4-months of age (Dale *et al.*, 2012, Shen *et al.*, 2011). Thus we analyzed motor coordination defects on symptomatic, 6-month-old hNF-L^{E396K} and hNF-L control mice. 6-month-old mice were trained for 5 days to walk on three progressively smaller circular wooden beams (5, 2.5 and 1cm diameter) 120 cm in length, suspended 50 cm from a bedding surface. During training, mice walked on each of the three beams for 3 minutes with at least 20 minutes of rest. After training, experiments were performed on the smallest beam, with markings in 5cm increments along the beam. Escape from beam was obstructed at each end. A digital camera was placed both perpendicular and parallel to the beam allowing for delineation of walking speed and foot slips, respectively. Mice were tested in three trials per day for three consecutive days (day 1, day 2, day 3) with at least 20 minutes of rest between trials. The number of falls, number of foot slips, total time walking, and the latency to fall within the 3-minute trials were scored for each day tested. The number of foot slips and falls were counted and normalized to amount of time walking per genotype per day tested. In addition, the average voluntary walking distance was measured using the 5cm intersection marks, and was used to calculate the average walking speed per genotype on the last day tested.

Thermal nociception

Response to thermal nociception was analyzed by Hargreaves assay (Hargreaves *et al.*, 1988) utilizing a Paw Thermal Stimulator System (Department of Anesthesiology, University of California, San Diego). 6-month-old mice were placed under wire cages on a glass surface that was maintained at 30°C. Latencies of limb withdrawal from a focused source of light were measured. Latencies of withdrawal were converted to temperatures by the construction of a standard curve using an attached thermocoupler under the glass surface.

Mechanical nociception

Threshold response to mechanical algesia was measured with a Dynamic Plantar Aesthesiometer (DPA) model # 37450 (Ugo Basile, Italy) in 6-month-old mice. Mice were set on a wire-mesh platform and allowed to habituate for at least 15 min. After habituation, the DPA monitored paw withdrawal thresholds. A metal filament was pushed against the

hind and front paws with an ascending linear force (10 g/s and 2 g/s, respectively) until a strong, immediate withdrawal occurred. Measurements were taken in triplicate and averages were reported as paw withdrawal thresholds in grams.

Immunohistochemistry

Muscle spindle analysis was performed on the Extensor Digitorum Longus (EDL) muscle in 2 and 6-month-old mice. Fresh EDL muscles were isolated and quickly flash frozen in liquid nitrogen-cooled isopentane. Unfixed 16μm transverse serial sections were made through the entire length of each muscle, and every 12th section was collected and stored at −20°C until further processing. Fresh unfixed sections were blocked in Hen serum for 1 hour at 4°C and then in in blocking solution (10% normal goat serum, 1% NP-40) for another hour at 4°C. Mouse monoclonal antibody against myosin heavy chain I (BA-D5-S, Developmental Studies Hybridoma Bank, University of Iowa, USA) in blocking solution (1:50) was applied to the sections and incubated overnight at 4°C. The sections were then washed 3× for 5 min with PBS, fixed with 4% PFA for 10 min at 4°C and washed again 3× for 5 min with PBS at room temperature. Sections were incubated in a chicken polyclonal antibody against neurofilament medium (CPCA-NF-M) in blocking solution (1:2000) at 4°C overnight to label axons followed by PBS washes 3× for 5 min at room temp. Subsequently, sections were washed for 5 min 3× with PBS, incubated with species-specific secondary antibodies that were conjugated with either Alexa Fluor 488 or 555 (Molecular Probes, Invitrogen) (1:500) diluted in blocking buffer, and washed again for 5min 3× with PBS. Slides were mounted in Vectashield with DAPI (Vector Labs, Burlingame, CA, USA), and imaged on a confocal microscope (Leica Microsystems, Inc, Model TPS SPE, Buffalo Grove, IL 60089.

Muscle Spindle Analysis

Individual muscle spindles were identified and traced through sequential serial sections. The area of each muscle spindle was measured in each serial section, and maximum, median, and minimum cross sectional areas were determined for each spindle. The approximate length of each muscle spindle was calculated by multiplying section thickness (16μm) by the number of spindle positive sections per individual spindle. Cross sectional area and calculated length were used to calculate muscle spindle volume. Measurements of all muscle spindles were averaged per genotype.

Statistical analysis

Average measurements for each observation from the balance beam results were analyzed for statistical significance by two-way repeated measures ANOVA followed by a Holm Sidak *post hoc* test (SigmaPlot, Systat Software Inc., San Jose, CA, US). Average measurements of axon counts, thermal nociception, mechanical nociception, auditory brainstem responses and muscle spindle analyses were all analyzed for statistical significance by Student's *t*-test.

Results

Reduced motor coordination in hNF-L^{E396K} mice

Time walking, distance walked, and walking speed—To analyze overall motor performance, we measured the total time spent walking (Fig. 1a), the distance walked (Fig. 1b) and the average walking speed (Fig. 1c) at each day tested. No significant differences were observed in any measurement between genotypes or across days tested.

Falls—The frequency of falls was also used to investigate motor coordination and balance (Carter *et al.*, 1999, Lepicard *et al.*, 2003). hNF-L^{E396K} mice had significantly ($F_{2,20} = 7.84$, $p < 0.001$) more falls (~3.0 fold) on day 1 compared to hNF-L controls (Fig. 2a). On days 2 and 3, the number of falls in hNF-L^{E396K} mice significantly dropped relative to day 1 ($F_{1,2} = 1.60$, $p = 0.0$, day 1 vs. day 2; $F_{1,2} = 1.60$ $p = 0.034$, day 1 vs. day 3) such that there was no difference between hNF-L^{E396K} and hNF-L mice. This suggested that hNF-L^{E396K} mice adapted to the balance beam. hNF-L control falls remained similar throughout all three days (Fig. 2a).

Foot Slips—Quantifying foot slips is an established method for analyzing motor coordination (Carter*et al.*, 1999, Stanley *et al.*, 2005), and increased slips reflect proprioceptive dysfunction (Muller*et al.*, 2008, Taylor *et al.*, 2001). A foot slip was classified as any event in which a paw fell off the top of the beam (Fig. 2b). The number of foot slips was quantified per trial on all test days. On day 1, hNF-L^{E396K} mice had ~ 2.0 times more foot slips compared to the hNF-L controls (Fig. 2c). However, these differences did not reach statistical significance. By day 2, the number of foot slips increased to ~2.5 times more than the controls (Fig. 2c), which was statistically significant ($F_{1,8} = 39.50$, $p = 0.031$). On day 3, the number of foot slips increased to ~3.5 times more than hNF-L controls (Fig. 2c). The number of foot slips on day 3 was significantly higher than controls ($F_{1, 8} = 39.50$ $p < 0.001$), and was also significant relative to hNF-L^{E396K} foot slips on day 2 ($F_{2,16} = 4.50$, $p = 0.020$) and day 1 ($F_{2,16} = 4.50$, $p = 0.002$). The number of foot slips did not change throughout the study for age matched hNF-L control mice (Fig. 2c). Taken together these analyses suggested that symptomatic hNF-L^{E396K} mice developed alterations in motor coordination consistent with loss of joint position sense.

Attenuated response to mechanical but not thermal nociception in hNF-L^{E396K} mice

We utilized two different paradigms to analyze nociception and target specific sensory axons in 6-month-old hNF-L and hNF-L^{E396K} mice: mechanical (group II, large myelinated axons) (Fig. 3) and thermal nociception (group III and IV, and unmyelinated) (Fig. 4). hNF-L^{E396K} mice required significantly more force to elicit a response in both the right hind ($p = 0.001$) (Fig. 3a) and left hind ($p = 0.013$) (Fig. 3b) paws compared to hNF-L controls. No differences were observed in evoked response in either right (Fig. 3c) or left front (Fig. 3d) paw. We analyzed thermal nociception by Hargreaves assay (Fig. 4). No differences were found in temperature threshold required to elicit a response (Fig. 4a – 4d), suggesting that reduction in mechanical nociception was not due to a generalized reduction in nociception. Taken together these results indicate that hNF-L^{E396K} mice develop deficits in large sensory axon function without altered function of small diameter sensory axons.

Progression from pre-symptomatic to symptomatic correlated with loss of large diameter sensory axons in hNF-L^{E396K} mice

Increased number of foot slips and decreased sensitivity to touch suggested alterations in proprioceptive and mechanoreceptive sensory neurons, which are large myelinated (>5 μm) sensory axons (Casellini & Vinik, 2007, Tourtellotte & Milbrandt, 1998). In 2-month-old hNF-L^{E396K} mice, the number of small (≤ 5μm) (Fig. 5a) and large (>5μm) (Fig. 5b) diameter axons was indistinguishable from age matched hNF-L controls. Aging from 2 to 6 months resulted in a reduction of ~300 small sensory axons in both hNF-L and hNF-L^{E396K} mice (Fig. 5c). Concomitantly, the number of large sensory axons increased by ~300 axons in hNF-L control mice (Fig. 5d). However, there was no increase in the number of large diameter sensory axons in 6-month-old hNF-L^{E396K} mice resulting in significantly fewer large sensory axons relative to age matched hNF-L controls (Fig. 5d), which is consistent with previous data showing a decrease (non-significant) of similar magnitude in the total number of sensory axons in symptomatic hNF-L^{E396K} mice (Shen *et al.*, 2011). Thus, our current analysis demonstrates that progressing from pre-symptomatic to symptomatic was associated with a specific loss of ~300 (~ 50%) large diameter sensory axons in hNF-L^{E396K} mice.

Muscle spindles cross sectional area and volume were reduced prior to disease onset in CMT2E mice

To determine if the loss of large diameter sensory axons was associated with alterations in muscle spindle number or morphology we analyzed muscle spindles from the EDL muscle. In each muscle section, several muscle spindles were identified (Fig. 6a). Each muscle spindle was then traced (as illustrated in Fig. 6b) to count the total number of muscle spindles in each muscle. No differences in muscle spindle number were found in 2 or 6-month-old hNF-L^{E396K} mice compared to age matched hNF-L controls (Fig. 6c).

The maximum ($p = 0.032$) (Fig. 7a), median ($p = 0.040$) (Fig. 7b), and minimum ($p = 0.010$) (Fig. 7c) cross sectional area were significantly reduced in 2-month-old hNF-L^{E396K} mice. In 6-month-old hNF-L^{E396K}, the maximum ($p = 0.341$) (not significant) (Fig. 7d), median ($p = 0.001$) (Fig. 7e) and minimum ($p = 0.018$) (Fig. 7f) cross sectional area were reduced in 6-month-old hNF-L^{E396K} mice compared to age matched hNF-L controls.

Muscle spindle length calculations revealed no difference in muscle spindle length between 2-month-old hNF-L^{E396K} (Fig. 8a) or 6-month-old hNF-L^{E396K} (Fig. 8b) and age matched hNF-L controls.

Utilizing the maximum area, minimum area, and length data we calculated the volume occupied by each muscle spindle. Our results revealed a significant decrease in muscle spindle volume of ~25% in 2-month-old (Fig. 8c) ($p = 0.027$) and ~26% in 6-month-old (Fig. 8d) ($p = 0.018$) hNF-L^{E396K} mice compared to the corresponding age matched controls. Taken together these data suggested that alterations in muscle spindle morphology preceded the loss of large diameter sensory axons in hNF-L^{E396K} mice.

Discussion

Expressing hNF-L^{E396K} in mice recapitulated many of the phenotypes observed in patients (Dale *et al.*, 2012, Shen *et al.*, 2011, Villalon *et al.*, 2015). The first overt phenotype observed in hNF-L^{E396K} mice was reduced ability to spread toes and reduced ability to abduct hind limbs, which was visible in ~4 month old mice (Shen *et al.*, 2011). This initial phenotype was suggestive of sensorimotor defects, but does not identify the site of pathogenesis. Our analyses have identified alterations that occur before onset of aberrant hind limb posture. At one month, neurofilament accumulations were visible in motor neuron cell bodies (Shen *et al.*, 2011). Ectopic accumulations persisted to 13 months, but were not progressive (Shen *et al.*, 2011). At two months, muscle spindle cross sectional area and volume were reduced, and axon diameter was reduced in gamma motor neurons (Shen *et al.*, 2011). These early alterations support pathogenesis within sensorimotor systems with predominant involvement of the proprioceptive system.

Altered motor function could contribute to many of the subsequent phenotypes. Reduced hind limb abduction is a gross measurement of sensorimotor function that could be explained by muscle weakness due to altered motor function (Clark, 2009). Motor coordination was compromised in freely ambulating hNF-L^{E396K} mice on a flat surface, which included left hind limb drag (Dale *et al.*, 2012). Foot drop is associated with muscle weakness (Bird, 1993a, Bird, 1993b). Muscle atrophy could directly result from reduced motor function (Akay, 2014, Boillee *et al.*, 2006) or indirectly from reduced voluntary activity (Clark, 2009), which was observed in hNF-L^{E396K} mice (Shen *et al.*, 2011).

Sensory dysfunction observed in hFN-L^{E396K} mice was specific to functions mediated by large diameter sensory axons. Increased number of foot slips on balance beam suggested possible dysfunction of group Ia or Ib sensory axons, which are large diameter sensory axons that transmit proprioception and joint position sense, respectively (Gilman, 2002). Furthermore, sensitivity to mechanical stimulation suggested altered function in group II sensory axons, which are also large sensory axons (Casellini & Vinik, 2007). However, functions mediated by unmyelinated axons, thermal nociception (Yeomans *et al.*, 1996, Yeomans & Proudfit, 1996), and small, myelinated axons, auditory brainstem responses (Supplementary Fig. 1) (Gleich & Wilson, 1993), were unaltered suggesting normal axonal function. Furthermore, morphological analysis of sensory axons supported large axon specificity, and identified a population of late developing sensory axons that were particularly vulnerable. Quantification of sensory axons at 2- and 6-months in hNF-L mice suggested an age related expansion in axonal diameter resulting in an increased number of large axons by ~300 axons. hNF-L^{E396K} mice also had a reduction in the number of small sensory axons, but the number of large diameter axons failed to increase suggesting loss of ~300 large sensory axons. Thus, functional deficits and morphological alterations indicated that hNF-L^{E396K}-linked CMT2E primarily affected sensory systems that utilize large diameter axons.

Muscle spindle cross sectional area and volume were significantly reduced in 2-month-old hNF-L^{E396K} mice. Loss of large sensory axons occurred subsequent to muscle spindle alterations. Moreover, gamma motor axon diameter was also reduced prior to onset of

aberrant hind limb posture (Shen *et al.*, 2011). It is possible that reduced function and altered morphology of muscle spindles in hNF-L^{E396K} mice resulted in secondary loss of large sensory axons and reduced gamma motor axon diameter. While the phenotype is much more extreme than the phenotype observed in hNF-L^{E396K} mice, muscle spindle agenesis resulted in secondary loss of large myelinated sensory and gamma motor axons during development in Egr3$^{-/-}$ mice (Tourtellotte & Milbrandt, 1998). However, further analysis is required to determine cause and effect in hNF-L^{E396K} mice, as muscle spindles do form in hNF-L^{E396K} mice.

Approximately 60 genes with over 900 unique mutations have been linked to a type of CMT (Bouhy & Timmerman, 2013). Given the large number of genes, it is unclear how mutations in such a wide array of genes that are expressed in different cell types leads to similar clinical presentations. Analysis of rodent models may begin to offer insights into convergence of disease phenotypes. Previous analyses of several CMT rodent models suggest early alterations in sensory systems (Achilli *et al.*, 2009, D'ydewalle *et al.*, 2011, Gillespie *et al.*, 2000, Lee *et al.*, 2013, Sereda *et al.*, 1996). Our analyses of hNF-L^{E396K} mice suggest early changes in sensorimotor systems with predominant involvement of the proprioceptive system. Therefore, early and selective dysfunction in proprioceptive sensory systems might provide a unifying hypothesis of disease pathogenesis in CMT. Given the heterogeneity of disease onset even within families with the same mutation (Berciano *et al.*, 2015, Züchner *et al.*, 2004), investigating proprioceptive system defects might be a useful diagnostic tool for early detection of pathologic changes in patients with family history of CMT. Moreover, specific alterations in proprioceptive systems observed prior to the onset of CMT-like pathology suggest that early intervention with therapies designed to enhance or maintain proprioception could be of significant therapeutic value to CMT patients.

Supplementary Material

Refer to Web version on PubMed Central for supplementary material.

Acknowledgements

This work was supported by Grants from National Institutes of Health [grant number NS060073], Charcot-Marie-Tooth Association [grant number C00014627], and Missouri Spinal Cord Injury/Disease Research Program to MLG. Salary support for MLG was provided by the University of Missouri and the C. S. Bond Life Sciences Center. JMD was supported by an ARRA supplement to T32 GM008396. HS was supported by Charcot-Marie-Tooth Association [grant number C00014627] to MLG. EV was supported by a training grant to Dr. Mark Hannink [grant number R25 GM056901]. DL was funded by a Post-baccalaureate Research Education Program grant to Drs. John David and Chris Hardin [grant number R25 GM641-20-7]. DDW was funded by an R01 grant from the NIAMS [grant number R01 AR067450].

References

Achilli F, Bros-Facer V, Williams HP, Banks GT, AlQatari M, Chia R, Tucci V, Groves M, Nickols CD, Seburn KL, Kendall R, Cader MZ, Talbot K, van Minnen J, Burgess RW, Brandner S, Martin JE, Koltzenburg M, Greensmith L, Nolan PM, Fisher EM. An ENU-induced mutation in mouse glycyl-tRNA synthetase (GARS) causes peripheral sensory and motor phenotypes creating a model of Charcot-Marie-Tooth type 2D peripheral neuropathy. Disease models & mechanisms. 2009; 2:359–373. [PubMed: 19470612]

Adebola AA, Di Castri T, He CZ, Salvatierra LA, Zhao J, Brown K, Lin CS, Worman HJ, Liem RK. Neurofilament Light Polypeptide Gene N98S Mutation in Mice Leads to Neurofilament Network Abnormalities and a Charcot-Marie-Tooth Type 2E Phenotype. Human molecular genetics. 2015; 24:2163–2174. [PubMed: 25552649]

Akay T. Long-term measurement of muscle denervation and locomotor behavior in individual wild-type and ALS model mice. J Neurophysiol. 2014; 111:694–703. [PubMed: 24174653]

Berciano J, Garcia A, Peeters K, Gallardo E, De Vriendt E, Pelayo-Negro AL, Infante J, Jordanova A. NEFL E396K mutation is associated with a novel dominant intermediate Charcot-Marie-Tooth disease phenotype. J Neurol. 2015; 262:1289–1300. [PubMed: 25877835]

Bird, TD. Charcot-Marie-Tooth Neuropathy Type 1. Pagon, RA.Bird, TD.Dolan, CR., Stephens, K., editors. GeneReviews; Seattle (WA): 1993a.

Bird, TD. Charcot-Marie-Tooth Neuropathy Type 2. Pagon, RA.Bird, TD.Dolan, CR., Stephens, K., editors. GeneReviews; Seattle (WA): 1993b.

Boillee S, Yamanaka K, Lobsiger CS, Copeland NG, Jenkins NA, Kassiotis G, Kollias G, Cleveland DW. Onset and progression in inherited ALS determined by motor neurons and microglia. Science. 2006; 312:1389–1392. [PubMed: 16741123]

Bouhy D, Timmerman V. Animal models and therapeutic prospects for Charcot-Marie-Tooth disease. Ann Neurol. 2013; 74:391–396. [PubMed: 23913540]

Butinar D, Starr A, Zidar J, Koutsou P, Christodoulou K. Auditory nerve is affected in one of two different point mutations of the neurofilament light gene☆. Clinical Neurophysiology. 2008; 119:367–375. [PubMed: 18023247]

Carter RJ, Lione LA, Humby T, Mangiarini L, Mahal A, Bates GP, Dunnett SB, Morton AJ. Characterization of progressive motor decificts in mice transgenic for the human huntington's disease mutation. The Journal of Neuroscience. 1999; 19:3248–3257. [PubMed: 10191337]

Casellini CM, Vinik AI. Clinical manifestations and current treatment options for diabetic neuropathies. Endocrinology Practice. 2007; 13:550–566.

Clark BC. In vivo alterations in skeletal muscle form and function after disuse atrophy. Med Sci Sports Exerc. 2009; 41:1869–1875. [PubMed: 19727027]

d'Ydewalle C, Krishnan J, Chiheb DM, Van Damme P, Irobi J, Kozikowski AP, Vanden Berghe P, Timmerman V, Robberecht W, Van Den Bosch L. HDAC6 inhibitors reverse axonal loss in a mouse model of mutant HSPB1-induced Charcot-Marie-Tooth disease. Nat Med. 2011; 17:968–974. [PubMed: 21785432]

Dale JM, Villalon E, Shannon SG, Barry DM, Markey RM, Garcia VB, Garcia ML. Expressing hNF-LE397K results in abnormal gaiting in a transgenic model of CMT2E. Genes, brain, and behavior. 2012; 11:360–365.

Dequen F, Filali M, Lariviere RC, Perrot R, Hisanaga S, Julien JP. Reversal of neuropathy phenotypes in conditional mouse model of Charcot-Marie-Tooth disease type 2E. Human molecular genetics. 2010; 19:2616–2629. [PubMed: 20421365]

Elbracht M, Senderek J, Schara U, Nolte K, Klopstock T, Roos A, Reimann J, Zerres K, Weis J, Rudnik-Schoneborn S. Clinical and morphological variability of the E396K mutation in the neurofilament light chain gene in patients with Charcot-Marie-Tooth disease type 2E. Clin Neuropathol. 2014; 33:335–343. [PubMed: 24887401]

Filali M, Dequen F, Lalonde R, Julien JP. Sensorimotor and cognitive function of a NEFL(P22S) mutant model of Charcot-Marie-Tooth disease type 2E. Behav Brain Res. 2011; 219:175–180. [PubMed: 21168446]

Fridman V, Bundy B, Reilly MM, Pareyson D, Bacon C, Burns J, Day J, Feely S, Finkel RS, Grider T, Kirk CA, Herrmann DN, Laura M, Li J, Lloyd T, Sumner CJ, Muntoni F, Piscosquito G, Ramchandren S, Shy R, Siskind CE, Yum SW, Moroni I, Pagliano E, Zuchner S, Scherer SS, Shy ME, Inherited Neuropathies C. CMT subtypes and disease burden in patients enrolled in the Inherited Neuropathies Consortium natural history study: a cross-sectional analysis. Journal of neurology, neurosurgery, and psychiatry. 2015; 86:873–878.

Gillespie CS, Sherman DL, Fleetwood-Walker SM, Cottrell DF, Tait S, Garry EM, Wallace VC, Ure J, Griffiths IR, Smith A, Brophy PJ. Peripheral demyelination and neuropathic pain behavior in periaxin-deficient mice. Neuron. 2000; 26:523–531. [PubMed: 10839370]

Gilman S. Joint position sense and vibration sense: anatomical organisation and assessment. Journal of neurology, neurosurgery, and psychiatry. 2002; 73:473–477.

Gleich O, Wilson S. The diameters of guinea pig auditory nerve fibres: distribution and correlation with spontaneous rate. Hear Res. 1993; 71:69–79. [PubMed: 7509334]

Hargreaves K, Dubner R, Brown F, Flores C, Joris J. A new and sensitive method for measuring thermal nociception in cutaneous hyperalgesia. Pain. 1988; 32:77–88. [PubMed: 3340425]

Lee SM, Sha D, Mohammed AA, Asress S, Glass JD, Chin LS, Li L. Motor and sensory neuropathy due to myelin infolding and paranodal damage in a transgenic mouse model of Charcot-Marie-Tooth disease type 1C. Hum Mol Genet. 2013; 22:1755–1770. [PubMed: 23359569]

Lepicard EM, Venault P, Negroni J, Perez-Diaz F, Joubert C, Nosten-Bertrand M, Berthoz A, Chapouthier G. Posture and balance responses to a sensory challenge are related to anxiety in mice. Psychiatry Research. 2003; 118:273–284. [PubMed: 12834821]

Mersiyanova IV, Perepelov AV, Polyakov AV, Sitnikov VF, Dadali EL, Oparin RB, Petrin AN, Evgrafov OV. A new variant of Charcot-Marie-Tooth disease type 2 is probably the result of a mutation in the neurofilament-light gene. American journal of human genetics. 2000; 67:37–46. [PubMed: 10841809]

Muller KA, Ryals JM, Feldman EL, Wright DE. Abnormal muscle spindle innervation and large-fiber neuropathy in diabetic mice. Diabetes. 2008; 57:1693–1701. [PubMed: 18362211]

Pareyson D, Scaioli V, Laurà M. Clinical and electrophysiological aspects of Charcot-Marie-Tooth disease. Neuromolecular Med. 2006; 8:3–22. [PubMed: 16775364]

Pisciotta C, Bai Y, Brennan KM, Wu X, Grider T, Feely S, Wang S, Moore S, Siskind C, Gonzalez M, Zuchner S, Shy ME. Reduced neurofilament expression in cutaneous nerve fibers of patients with CMT2E. Neurology. 2015; 85:228–234. [PubMed: 26109717]

Sereda M, Griffiths I, Puhlhofer A, Stewart H, Rossner MJ, Zimmerman F, Magyar JP, Schneider A, Hund E, Meinck HM, Suter U, Nave KA. A transgenic rat model of Charcot-Marie-Tooth disease. Neuron. 1996; 16:1049–1060. [PubMed: 8630243]

Shen H, Barry DM, Dale JM, Garcia VB, Calcutt NA, Garcia ML. Muscle pathology without severe nerve pathology in a new mouse model of Charcot-Marie-Tooth disease type 2E. Human molecular genetics. 2011; 20:2535–2548. [PubMed: 21493625]

Stanley JL, Lincoln RJ, Brown TA, McDonald LM, Dawson GR, Reynolds DS. The mouse beam walking assay offers improved sensitivity over the mouse rotarod in determining motor coordination deficits induced by benzodiazepines. J Psychopharmacol. 2005; 19:221–227. [PubMed: 15888506]

Szigeti K, Lupski JR. Charcot-Marie-Tooth disease. Eur J Hum Genet. 2009; 17:703–710. [PubMed: 19277060]

Taylor MD, Vancura R, Patterson CL, Williams JM, Riekhof JT, Wright DE. Postnatal regulation of limb proprioception by muscle-derived neurotrophin-3. J Comp Neurol. 2001; 432:244–258. [PubMed: 11241389]

Tourtellotte WG, Milbrandt J. Sensory ataxia and muscle spindle agenesis in mice lacking the transcription factor Egr3. Nat Genet. 1998; 20:87–91. [PubMed: 9731539]

Villalon E, Dale JM, Jones M, Shen H, Garcia ML. Exacerbation of Charcot-Marie-Tooth type 2E neuropathy following traumatic nerve injury. Brain Res. 2015; 1627:143–153. [PubMed: 26423936]

Yeomans DC, Pirec V, Proudfit HK. Nociceptive responses to high and low rates of noxious cutaneous heating are mediated by different nociceptors in the rat: behavioral evidence. Pain. 1996; 68:133–140. [PubMed: 9252008]

Yeomans DC, Proudfit HK. Nociceptive responses to high and low rates of noxious cutaneous heating are mediated by different nociceptors in the rat: electrophysiological evidence. Pain. 1996; 68:141–150. [PubMed: 9252009]

Züchner S, Vorgerd M, Sindern E, Schröder JM. The novel neurofilament light (NEFL) mutation Glu397Lys is associated with a clinically and morphologically heterogeneous type of Charcot-Marie-Tooth neuropathy. Neuromuscular Disorders. 2004; 14:147–157. [PubMed: 14733962]

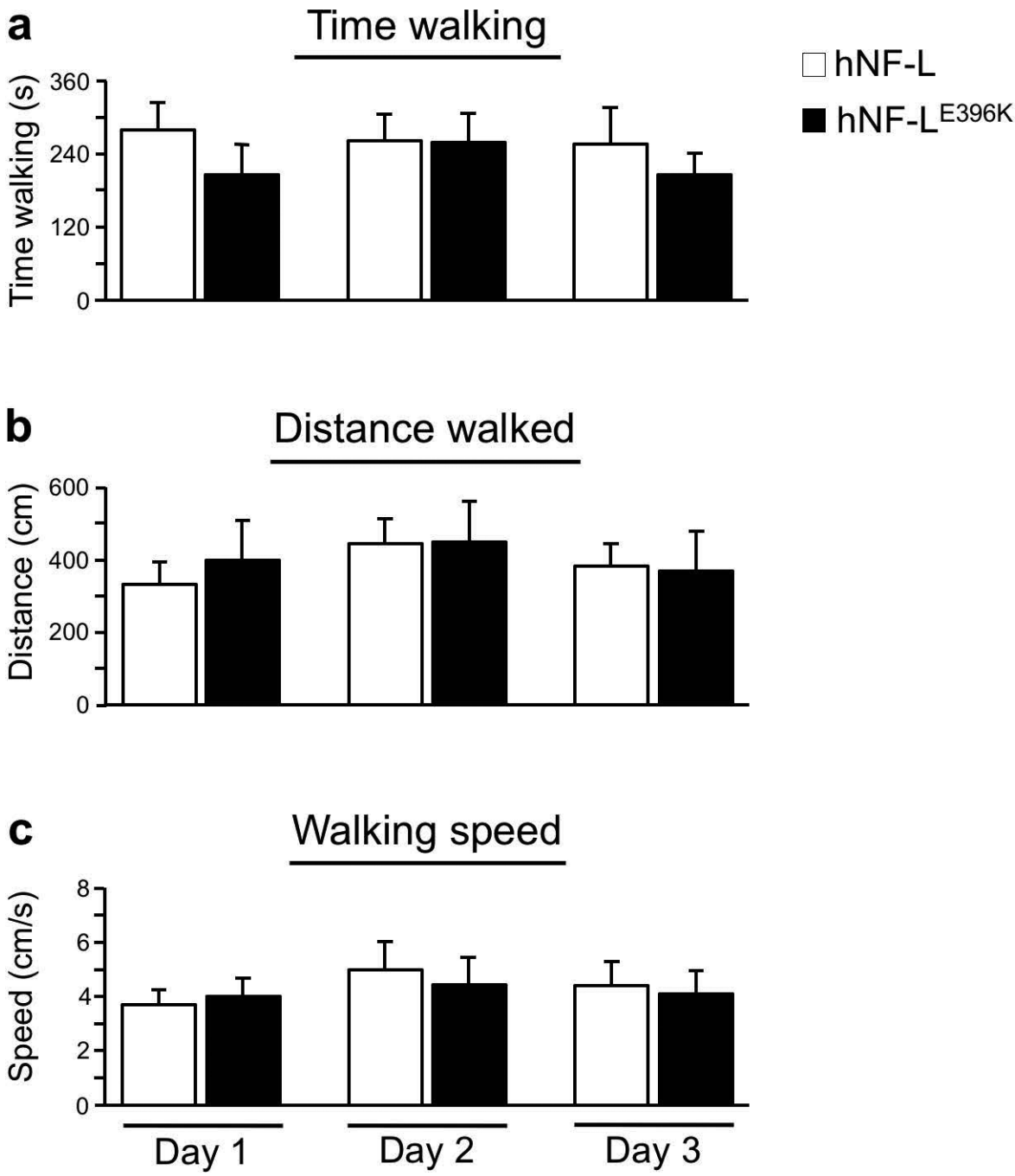

Fig. 1.

Ability to traverse the balance beam was not altered in symptomatic hNF-L^{E396K} mice. Ability to traverse the beam was analyzed by measuring total walking time, distance walked, and walking speed in 5 - 6-month-old hNF-L and hNF-L^{E396K} mice. No differences were observed in total walking time (a), distance walked (b) or walking speed (c) on any day between symptomatic hNF-L^{E396K} and hNF-L control mice. All observations were averaged per day per genotype, and analyzed for statistical significance by two-way repeated

measures ANOVA followed by a Holm Sidak post-hoc test for pairwise comparisons. Error bars = SEM. N = 6 for hNF-L and hNF-L^{E396K}.

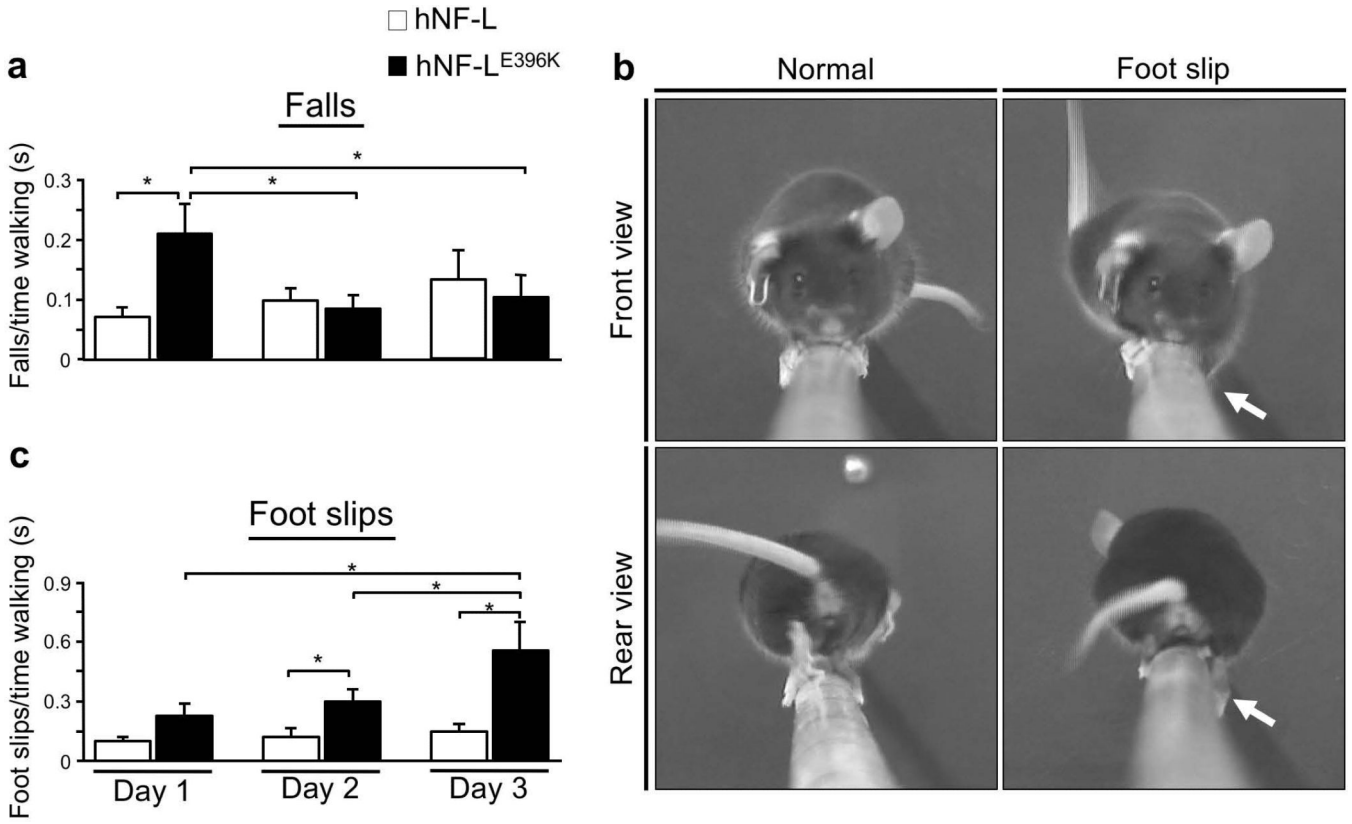

Fig. 2.

Motor coordination was reduced in symptomatic hNF-L^{E396K} mice. Motor coordination was analyzed by balance beam in 5 - 6-month-old hNF-L^{E396K} and hNF-L mice. (a) On day 1, symptomatic hNF-L^{E396K} mice had significantly more falls than aged matched hNF-L controls. However, by day 2 and 3, symptomatic hNF-L^{E396K} mice fell the same number of times as hNF-L control mice. (b) Illustration of a normal mouse on the balance beam (left) and a mouse experiencing a foot slip (right). A foot slip was considered any event when the foot fell below the top surface of the beam (arrows). (c) Symptomatic hNF-L^{E396K} mice had a progressive increase in the number of foot slips on the balance beam over the three consecutive days. All observations were averaged per day per genotype, and analyzed for statistical significance by two-way repeated measures ANOVA followed by a Holm Sidak post-hoc test for pairwise comparisons. Error bars = SEM. N = 6 for hNF-L and hNF-L^{E396K}. * = $p < 0.05$.

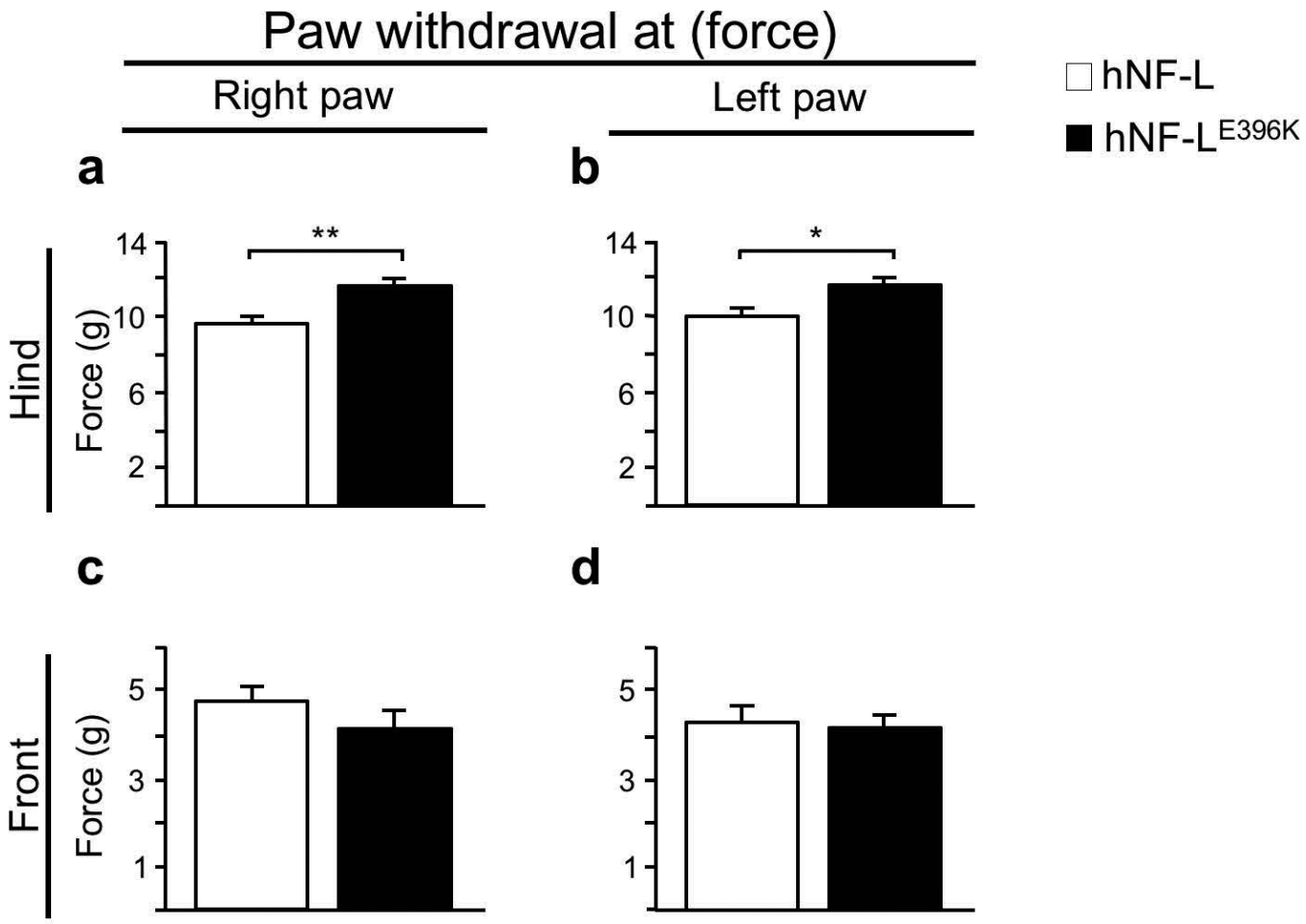

Fig. 3.

Sensitivity to mechanical stimulation was reduced in hind limbs of symptomatic hNF-L^{E396K} mice. Flexor withdrawal reflex was measured in 6-month-old hNF-L^{E396K} and hNF-L mice. (a and b) Grams of force required to elicit the withdrawal reflex was significantly higher in the right hind (a) and left hind (b) paws of symptomatic hNF-L^{E396K} mice compared to age matched hNF-L mice. (c and d) No differences were observed in the amount of force required to elicit a response in the right (c) or left (d) front paws. All observations were averaged per genotype, and analyzed for statistical significance by a Student's *t*-test. Error bars = SEM. N = 8 for hNF-L controls, and N = 15 for hNF-L^{E396K}. * = $p < 0.05$, ** = $p < 0.001$.

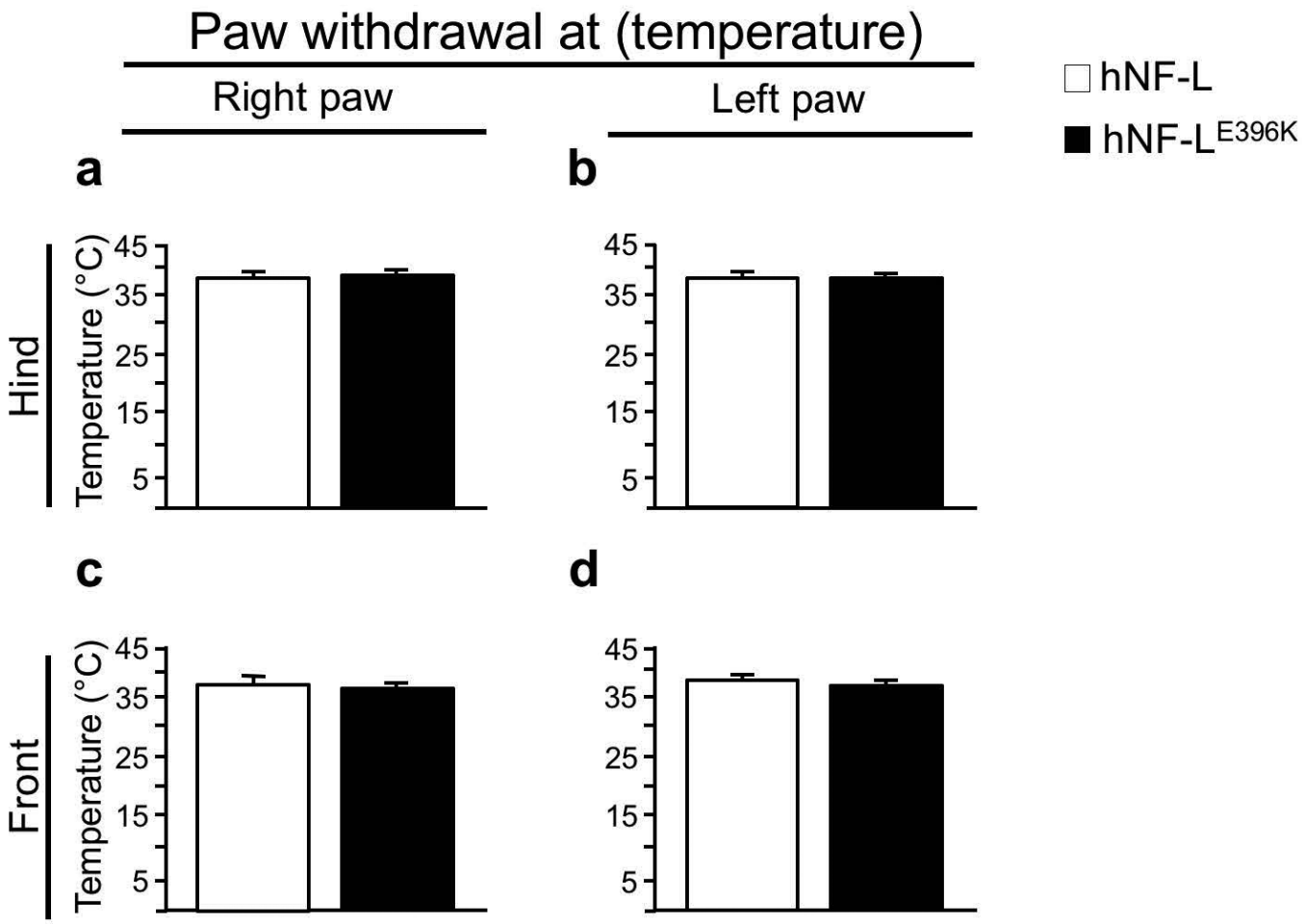

Fig. 4.

Sensitivity to thermal stimulation was not affected in symptomatic hNF-L^{E396K} mice. The flexor withdrawal reflex was further analyzed utilizing noxious thermal stimulation in 6-month-old hNF-L and hNF-L^{E396K} mice. (a, b, c, and d). No differences in response to noxious thermal stimulation were observed in the right hind (a), left hind (b), right front (c), or left front (d) paws between symptomatic hNF-L^{E396K} or hNF-L control mice. Measurements were averaged per paw and genotype, and analyzed for statistical significance using a Student's *t*-test. Error bars = SEM. N = 15 for hNF-L and N = 22 for hNF-L^{E396K}.

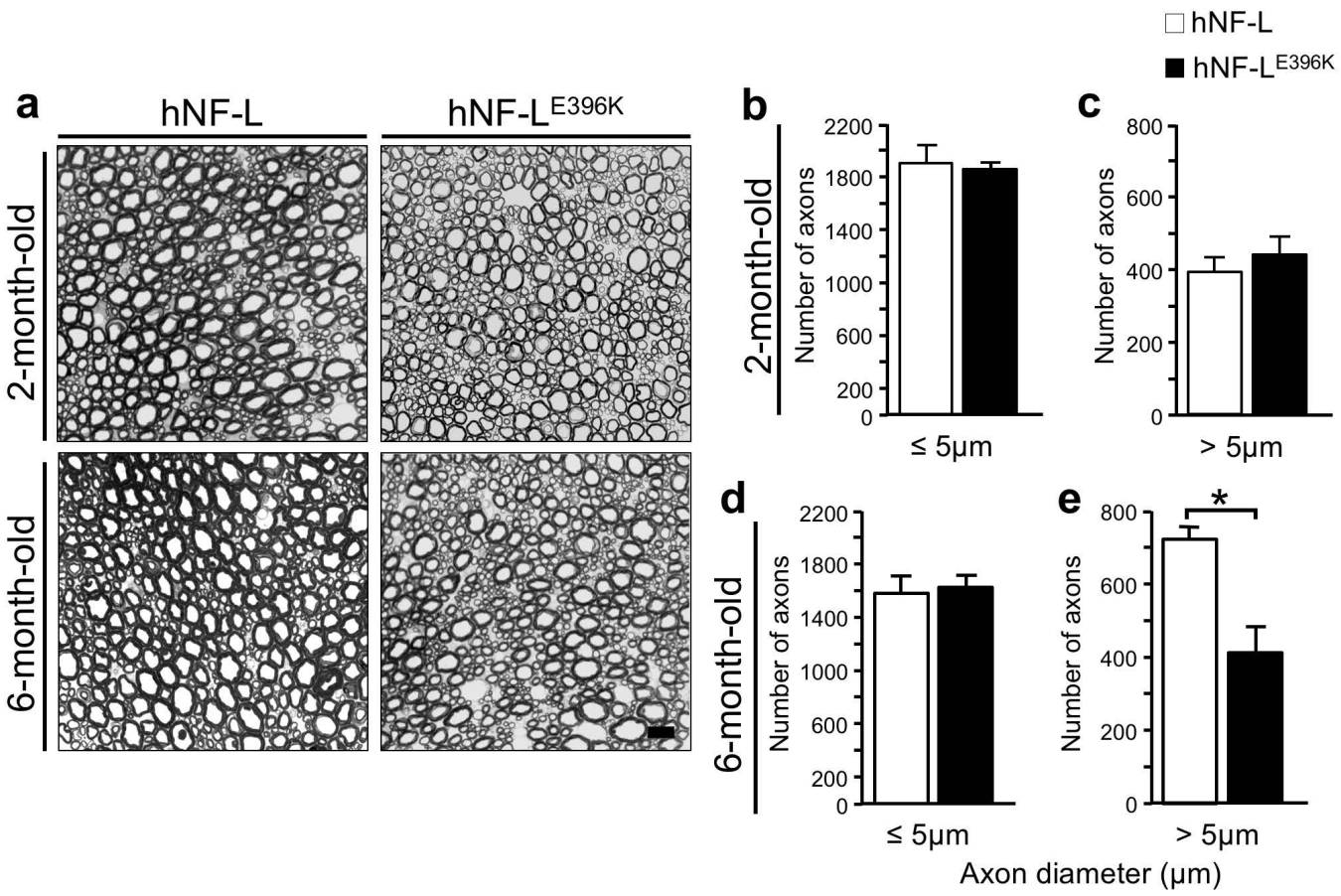

Fig. 5.

Progression from pre-symptomatic to symptomatic resulted in loss of large diameter sensory axons in hNF-L^{E396K} mice. Representative micrographs of hNF-L and hNF-L^{E396K} fifth lumbar sensory roots (scale bar = 10μm) (a). Fifth lumbar sensory root axons were divided into small (< 5μm) and large (> 5μm) diameter populations in 2-month-old and 6-month-old hNF-L and hNF-L^{E396K} mice. (b and c) The number of small (b) and large (c) diameter sensory axons was not different in pre-symptomatic hNF-L^{E396K} and age matched hNF-L controls. (d) In symptomatic hNF-L^{E396K} and age matched hNF-L mice, small diameter sensory axons were reduced by approximately 300 axons. As hNF-L and hNF-L^{E396K} both had reduced numbers, there was no difference in total number of small diameter axons. (e) In 6-month-old hNF-L mice, the number of large diameter axons was increased by approximately 300 axons. However, large diameter axons did not increase in symptomatic hNF-L^{E396K} mice resulting in a significant reduction in the total number of large diameter axons. Axon counts were averaged per genotype and analyzed for statistical significance by a Student's *t*-test. Error bars = SEM. N = 3 for 2-month-old hNF-L and hNF-L^{E396K}. N = 4 for 6-month-old hNF-L and hNF-L^{E396K}. * = $p < 0.05$.

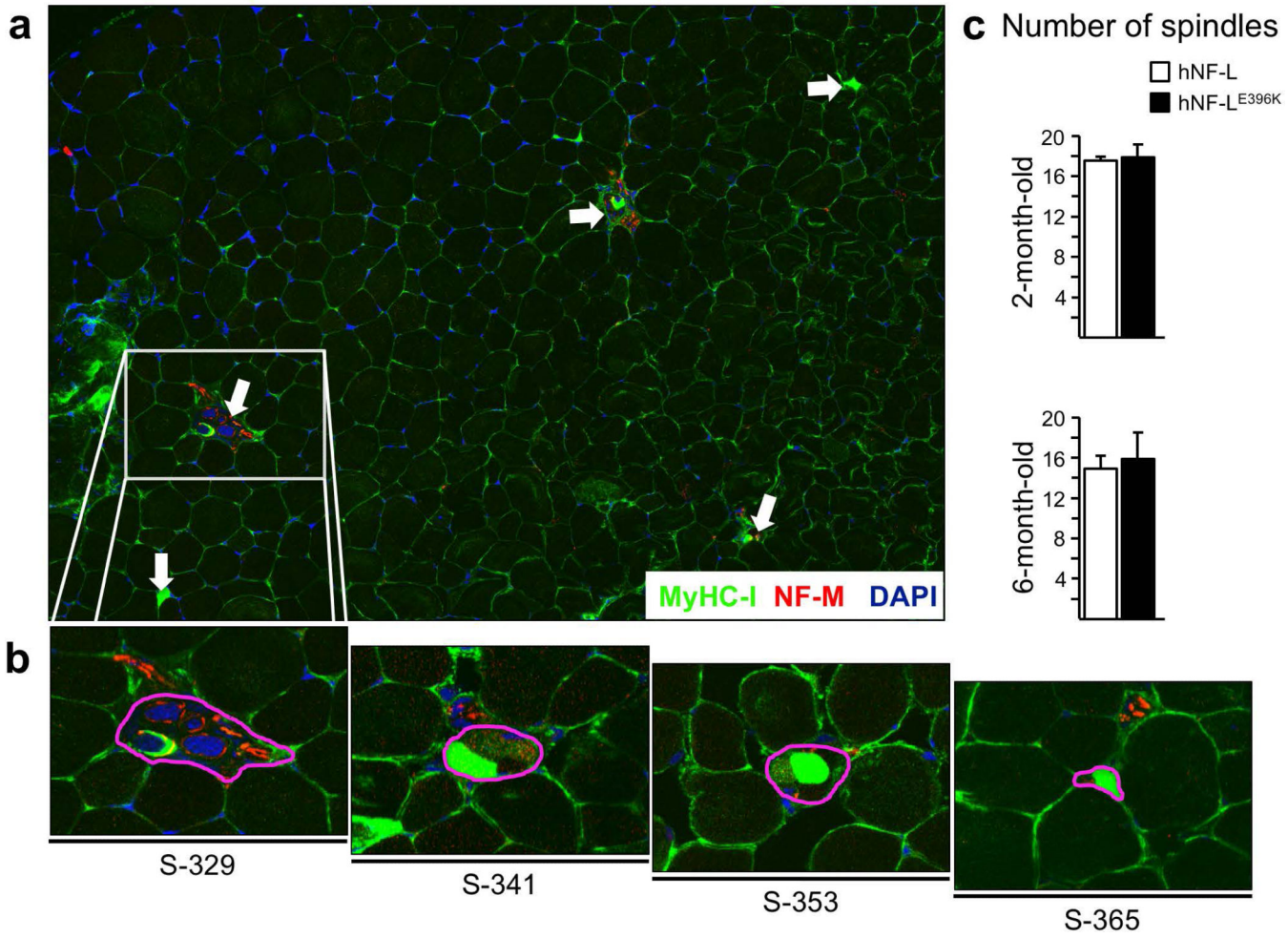

Fig. 6.

Muscle spindle number was unaffected in extensor digitorum longus muscles from pre-symptomatic and symptomatic hNF-L^{E396K} mice. (a) Extensor digitorum longus (EDL) muscles were serially sectioned (16μm), and every 12th serial section was immunostained using antibodies specific for myosin heavy chain type I (green) and neurofilament medium (red) to identify muscle spindles and associated axons (arrows point to individual muscle spindles). (b) Individual muscle spindles were traced through the sections they appeared in and the area they occupied was outlined for cross sectional area analyses. (c) Muscle spindles were counted in 2 and 6-month-old hNF-L and hNF-L^{E396K} mice. No difference was observed in muscle spindle number in pre-symptomatic or symptomatic hNF-L^{E396K} mice compared to respective age matched hNF-L controls. Muscle spindles were averaged per genotype and analyzed for statistical significance by a Student's *t*-test. Error bars = SEM. N = 3 for both hNF-L and hNF-L^{E396K}. S-329: section 329, S-341: section 341, etc.

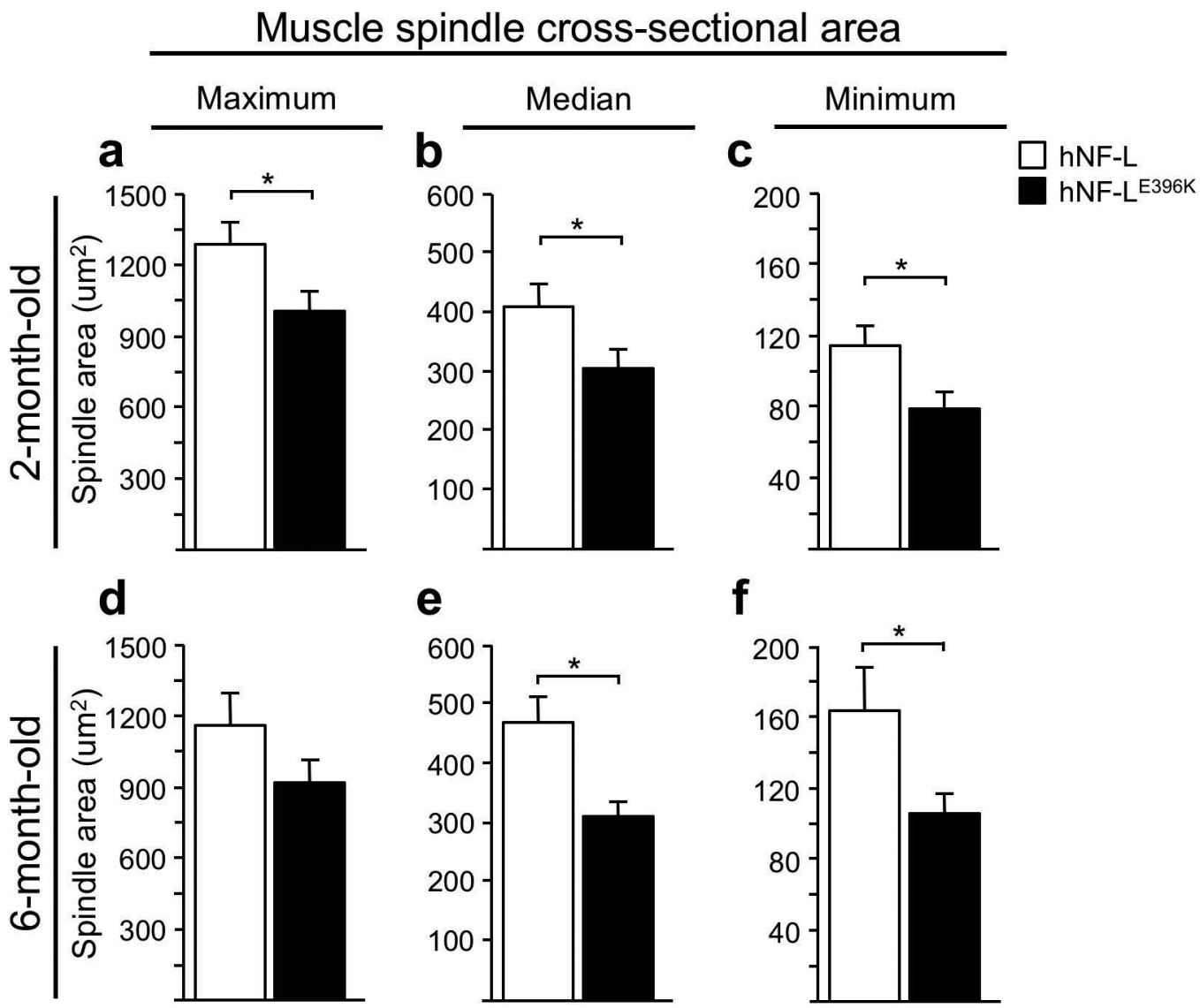

Fig. 7.

Muscle spindle cross sectional area was reduced in pre-symptomatic and symptomatic hNF-L^{E396K} mice. Muscle spindle cross sectional area was analyzed in 2 and 6-month-old hNF-L and hNF-L^{E396K} mice. (a, b, and c) Maximum (a), median (b), and minimum (c) muscle spindle cross sectional area was significantly reduced in pre-symptomatic hNF-L^{E396K} mice relative to age matched hNF-L controls. (d) Maximum cross sectional area was reduced in symptomatic hNF-L^{E396K} mice compared to age matched hNF-L controls. However, the differences did not reach statistical significance. (e and f) Median (e) and minimum (f) muscle spindle cross sectional area was significantly reduced in symptomatic hNF-L^{E396K} mice compared to age matched hNF-L controls. Averages per genotype were calculated from measurements of all counted muscle spindles, and analyzed for statistical significance by a Student's *t*-test. Error bars = SEM. N ≥ 15 for both hNF-L and hNF-L^{E396K}. * = $p < 0.05$.

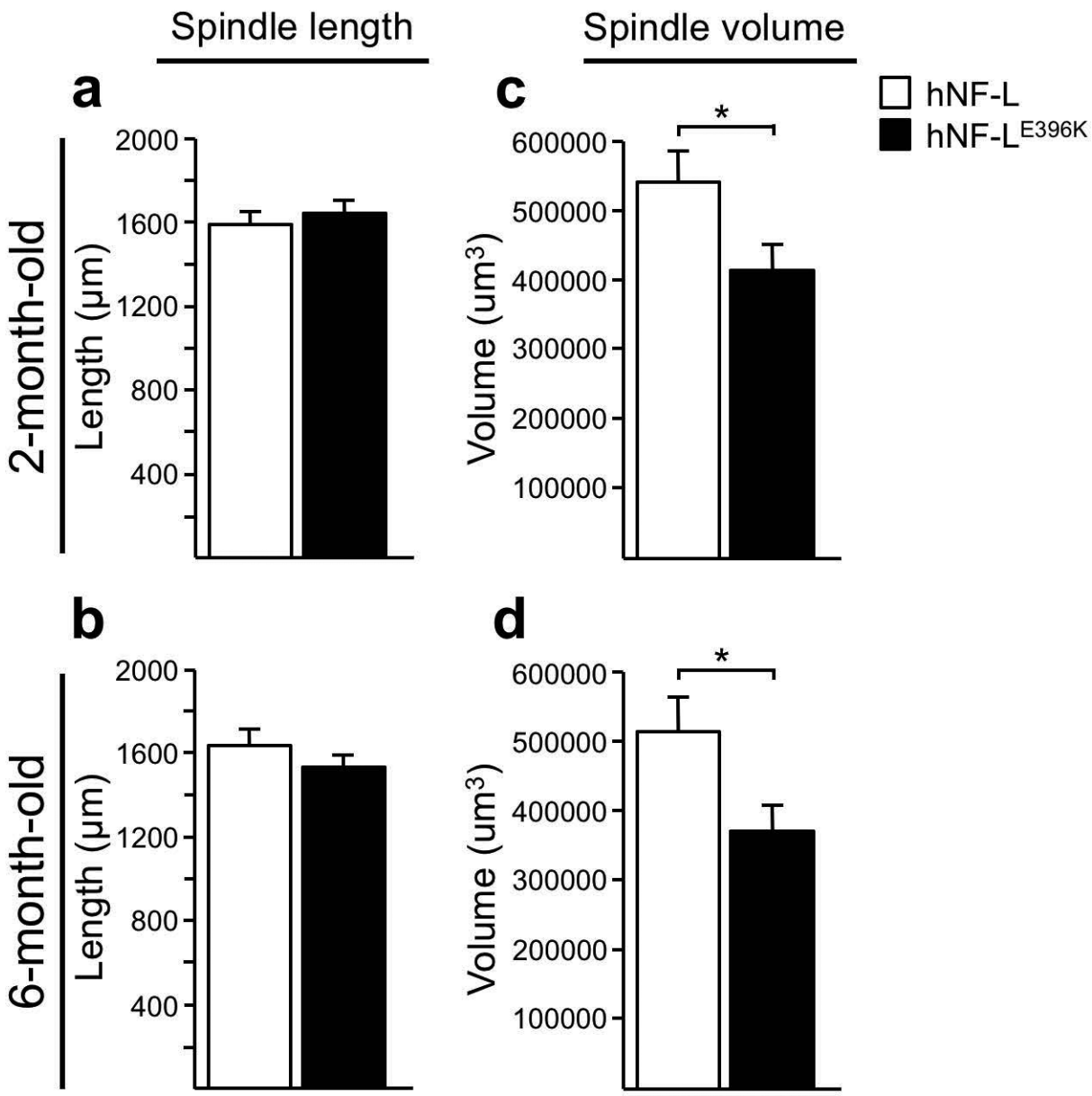

Fig. 8.

Muscle spindle volume was reduced in pre-symptomatic and symptomatic hNF-L^{E396K} mice. Muscle spindle length and volume were calculated in 2 and 6-month-old hNF-L and hNF-L^{E396K} mice. (a and b) Muscle spindle length was not different in pre-symptomatic (a) and symptomatic (b) hNF-L^{E396K} mice relative to age matched hNF-L controls. (c and d) There was a significant reduction in muscle spindle volume in pre-symptomatic (c) and symptomatic (d) hNF-L^{E396K} mice compared to age matched hNF-L controls. Averages per genotype were calculated from measurements of all counted muscle spindles, and analyzed for statistical significance by a Student's *t*-test. Error bars = SEM. N ≥ 15 for both hNF-L and hNF-L^{E396K}. * = $p < 0.05$.